

# Beyond Boundaries: Leveraging Vision Foundation Models for Source-Free Object Detection

Huizai Yao<sup>1</sup>, Sicheng Zhao<sup>2</sup>, Pengteng Li<sup>1</sup>, Yi Cui<sup>1</sup>, Shuo Lu<sup>3</sup>,  
Weiyu Guo<sup>1</sup>, Yunfan Lu<sup>1</sup>, Yijie Xu<sup>1</sup>, Hui Xiong<sup>1,4\*</sup>

<sup>1</sup> Thrust of Artificial Intelligence, The Hong Kong University of Science and Technology (Guangzhou), China

<sup>2</sup> Department of Psychological and Cognitive Sciences, Tsinghua University, China

<sup>3</sup> NLPR & MAIS, Institute of Automation, Chinese Academy of Sciences, China

<sup>4</sup> Department of Computer Science and Engineering, The Hong Kong University of Science and Technology, Hong Kong SAR, China

huizai.yao@connect.hkust.edu.cn

## Abstract

Source-Free Object Detection (SFOD) aims to adapt a source-pretrained object detector to a target domain without access to source data. However, existing SFOD methods predominantly rely on internal knowledge from the source model, which limits their capacity to generalize across domains and often results in biased pseudo-labels, thereby hindering both transferability and discriminability. In contrast, Vision Foundation Models (VFM), pretrained on massive and diverse data, exhibit strong perception capabilities and broad generalization, yet their potential remains largely untapped in the SFOD setting. In this paper, we propose a novel SFOD framework that leverages VFM as external knowledge sources to jointly enhance feature alignment and label quality. Specifically, we design three VFM-based modules: (1) Patch-weighted Global Feature Alignment (PGFA) distills global features from VFM using patch-similarity-based weighting to enhance global feature transferability; (2) Prototype-based Instance Feature Alignment (PIFA) performs instance-level contrastive learning guided by momentum-updated VFM prototypes; and (3) Dual-source Enhanced Pseudo-label Fusion (DEPF) fuses predictions from detection VFM and teacher models via an entropy-aware strategy to yield more reliable supervision. Extensive experiments on six benchmarks demonstrate that our method achieves state-of-the-art SFOD performance, validating the effectiveness of integrating VFM to simultaneously improve transferability and discriminability.

**Code** — [https://github.com/HuizaiVictorYao/VFM\\_SFOD](https://github.com/HuizaiVictorYao/VFM_SFOD)

## 1 Introduction

Object detection, a fundamental task in computer vision that aims to accurately localize and classify objects in images or videos, has witnessed rapid advancements in the past decade. While various detectors have been extensively developed, they typically assume that training and testing data (i.e., source and target domains) are independently and identically distributed (*i.i.d.*). This assumption often fails in real-world scenarios, leading to a significant drop in performance when these detectors are directly applied to unseen domains.

\*Corresponding Author (xionghui@ust.hk).

Copyright © 2026, Association for the Advancement of Artificial Intelligence (www.aaai.org). All rights reserved.

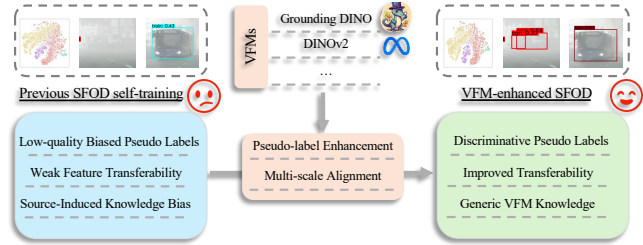


Figure 1: Illustration of our VFM-enhanced SFOD motivation. Our method leverages general VFM knowledge in VFM such as DINOv2 (visual encoder) and Grounding DINO (vision-language detector) to address pseudo-label bias and multi-scale feature misalignment, resulting in improved transferability and discriminability compared with previous self-training pipelines of SFOD.

To alleviate this issue, Domain Adaptive Object Detection (DAOD) has been widely studied. DAOD aims to transfer a detector trained on labeled source data to unlabeled target data. However, their dependence on source data limits their applicability in scenarios involving privacy, security, or data transmission constraints (Li et al. 2024a; Lu et al. 2025b; Zhao et al. 2023). To address this, Source-Free Object Detection (SFOD) has emerged as a promising alternative, aiming to adapt a source-pretrained detector to a target domain using only unlabeled target data (VS, Oza, and Patel 2023; Chu et al. 2023; Yoon et al. 2024; Hao, Forest, and Fink 2024; Khanh et al. 2024; Zhao et al. 2024a).

Previous research has identified two critical properties for effective cross-domain adaptation: transferability and discriminability (Kundu et al. 2022; Li et al. 2024a). Transferability ensures that feature representations remain domain-invariant, while discriminability guarantees separability between object categories. Despite this, current SFOD methods primarily focus on knowledge distillation within the teacher-student paradigm—through feature alignment (Li et al. 2022a), adversarial learning (Chu et al. 2023), or pseudo-label refinement (Chen, Wang, and Zhang 2023; Zhao et al. 2024a), without breaking out of the internal

semantic space provided by the source-pretrained detector. This closed-loop design fails to overcome the limitations of the original backbone, which often lacks semantic richness and precise decision boundaries, especially under large domain shifts. Consequently, both transferability and discriminability remain limited under domain shifts due to the restricted and homogeneous nature of internal representations in current SFOD approaches.

To address this, we turn to external knowledge sources, particularly Vision Foundation Models (VFM). These large-scale models, pretrained on massive and diverse data, offer powerful generalization and strong visual perception. Yet, their potential remains underexplored in the SFOD setting. VFM, including visual encoders such as DINOv2 (Oquab et al. 2023) and vision-language detectors such as Grounding DINO (Liu et al. 2024), provide rich, transferable features and robust semantic priors, making them well-suited to augment both feature representation and label quality under source-free constraints. Some recent methods have begun exploring the use of VFM in domain adaptation. For instance, DINO Teacher (DT)(Lavoie, Mahmoud, and Waslander 2025) aligns detector and VFM features but requires source data and supervision, violating the SFOD assumption. CODA(Li et al. 2024b) explores external detections to enhance discriminability in cloud deployment settings, but overlooks improvements to feature-level transferability. Thus, how to fully and effectively leverage VFM for improving SFOD in terms of discriminability and transferability remains an open and underexplored problem.

To tackle this challenge, we propose a novel VFM-enhanced SFOD framework, as illustrated in Fig. 2. Unlike previous SFOD approaches that suffer from low-quality pseudo-labels, weak transferability, and source-induced knowledge bias, our method incorporates VFM through three key modules to address these limitations. To enhance global feature-level transferability, we propose **Patch-weighted Global Feature Alignment (PGFA)**. This module improves feature transferability by aligning the student’s feature space with that of a VFM such as DINOv2 (Oquab et al. 2023), guided by patch-wise similarity weights. It encourages the student to learn from VFM’s rich, domain-agnostic representations. Considering the importance of instance features in object detection, we propose **Prototype-based Instance Feature Alignment (PIFA)**. This component constructs momentum-based prototypes from VFM features and performs contrastive learning at the instance level, enhancing fine-grained feature alignment and improving instance-level feature transferability and discriminability. To further improve pseudo-label discriminability in the self-training pipeline, we propose **Dual-source Enhanced Pseudo-label Fusion (DEPF)**. In DEPF, we fuse predictions from object detection VFM such as Grounding DINO (Liu et al. 2024) and the teacher model using instance-level uncertainty-weighted box fusion. This produces cleaner, more reliable supervision signals without relying solely on the biased teacher.

As shown in Fig. 1, the proposed framework bridges the gap between conventional SFOD and the rich representation space of VFM. By integrating pseudo-label enhancement,

global feature alignment, and instance-level alignment, our method significantly boosts both discriminability and transferability. The resulting detector benefits from the broad generalization capability of VFM and the structure-aware learning of the student-teacher paradigm.

Our main contributions are summarized as follows:

- We identify a key limitation in current SFOD methods: the underutilization of Vision Foundation Models. To this end, we propose a unified framework that integrates VFM to address both feature transferability and label discriminability.
- We design three lightweight but effective VFM-based components: **PGFA**, **PIFA**, and **DEPF**, which enhance global and instance-level alignment and improve pseudo-label quality through multi-source fusion, synergistically improve both discriminability and transferability.
- We conduct extensive experiments on multiple cross-domain object detection benchmarks. Results demonstrate that our method achieves state-of-the-art SFOD performance, validating the effectiveness of leveraging VFM for cross-domain adaptation.

## 2 Related Work

### 2.1 Domain Adaptive Object Detection

Domain Adaptive Object Detection (DAOD) aims to transfer detection knowledge from labeled source domains to unlabeled target domains. Prior methods leverage self-training with teacher-student models (Chen et al. 2022; Kennerley et al. 2024; Yao et al. 2021), fine-grained alignment via graph matching (Li, Liu, and Yuan 2022; Li et al. 2023b), and data augmentation or image translation for improved generalization (Liu et al. 2021a). More recently, Vision-Language or Foundation Models (VLMs/VFM) have been introduced to enhance semantic robustness (Li et al. 2023a, 2024a; Lavoie, Mahmoud, and Waslander 2025). However, most DAOD methods require access to source data, which conflicts with privacy constraints. In contrast, our work operates in a source-free setting, without using any labeled source images.

### 2.2 Source-Free Object Detection

SFOD (Source-Free Object Detection) aims to transfer a source pretrained model to unsupervised target domain without access to any source images. Previous SFOD approaches perform efficient knowledge transfer by techniques such as feature alignment (Li et al. 2022a; VS, Oza, and Patel 2023; Yao et al. 2025) or refined pseudo-labelling (Chen, Wang, and Zhang 2023; Zhang, Zhang, and Liu 2023; Zhao et al. 2024a). However, these methods operate on internal knowledge and limited decision boundary of source pretrained model, making the target performance rather limited. VG-DETR (Han, Wang, and Chen 2025) similarly employs VFM for semi-supervised SFOD, but uses feature clustering for pseudo-labeling, leading to lower efficiency and reliability. In contrast, our method considers the rapid development of VFM and leverages the rich semantic and broad decision boundary from VFM pretrained by large-scale data.

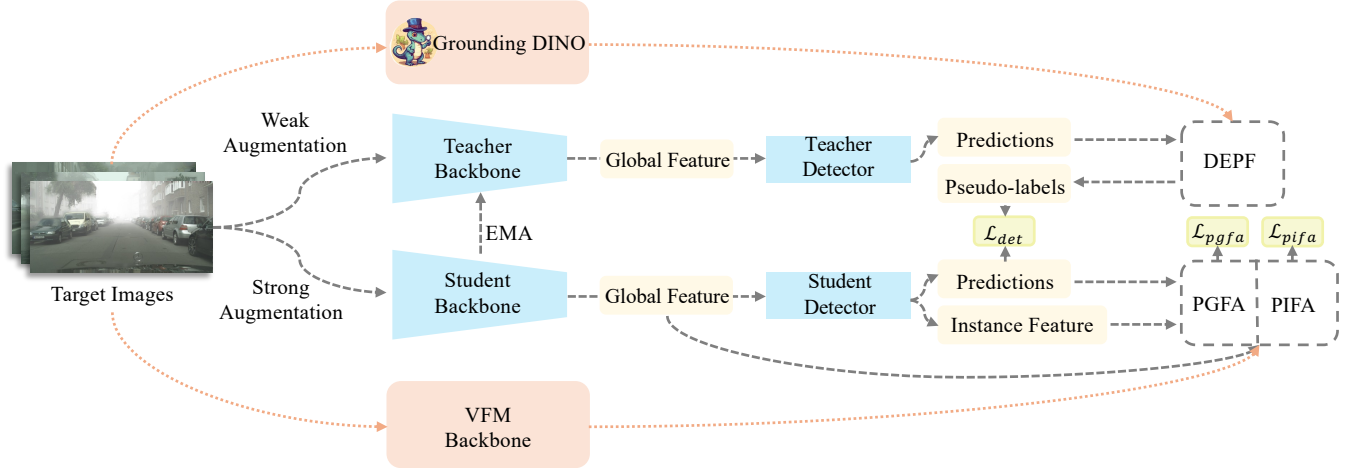


Figure 2: Overview of the proposed method. Unlabeled target images are fed into teacher and student models for self-training with detection loss. DEPF fuses teacher and Grounding DINO predictions to generate refined pseudo-labels, enhancing discriminability. PGFA and PIFA align multi-scale features from the student and VFM, leveraging the generic VFM space to improve transferability.

### 2.3 Vision Foundation Models

VFMs are large pre-trained models that provide a versatile foundation for vision tasks, offering broad generalization and easy adaptation via prompting or light tuning (Awais et al. 2025). Recent VFMs have shown promising performance on various vision tasks such as Segment Anything Model for segmentation (Kirillov et al. 2023), Grounding DINO for object detection (Liu et al. 2024), Depth Anything (Yang et al. 2024) and DINOv2 (Oquab et al. 2023) for depth estimation. Meanwhile, VLMs and MLLMs further extend this foundation to joint multimodal understanding (Lu et al. 2025a; Wu et al. 2025; Wang et al. 2025). In this work, we leverage the rich semantic prior and strong visual perception of VFMs to effectively enhance SFOD discriminability and transferability.

## 3 Method

### 3.1 Preliminaries

**Problem Setup.** In SFOD approaches, the main goal is to transfer a detection model  $\theta_S$  from source domain  $D_S$  and target domain  $D_T$  with unsupervised target dataset  $X_T = \{x_T^i\}_{i=1}^{N_T}$ . The source model is pretrained from source dataset  $X_S = \{x_S^i, y_S^i\}_{i=1}^{N_S}$  where each  $(x_S^i, y_S^i)$  is *i.i.d.* sampled from the source domain distribution  $D_S$ . Similarly, each  $x_T^i$  is *i.i.d.* sampled from  $D_T$  but the ground-truth label is unknown. Finally, the transferred detection model  $\theta_T : x_T \rightarrow y_p$  is of good cross-domain generalization and perform well on target domain.

**Mean Teacher Self-Training Pipeline.** Following previous approaches (Li et al. 2022a; VS, Oza, and Patel 2023), we adopt Mean Teacher (Tarvainen and Valpola 2017) framework as the baseline. Firstly, a teacher model  $\theta_{te}$  and a student model  $\theta_{st}$  is initialized by the same parameter of the source pretrained model. In the adaptation stage, a batch of

target samples is weakly and strongly augmented, and input to  $\theta_{te}$  and  $\theta_{st}$  respectively.  $\theta_{te}$  generates pseudo-labels as supervision signals for  $\theta_{st}$ , and  $\theta_{st}$  is updated with loss backpropagation.  $\theta_{te}$  does not update from backpropagation but an exponential moving average (EMA) from  $\theta_{st}$  parameters. This progress can be denoted as:

$$\begin{cases} \theta_{st} \leftarrow \theta_{st} + \eta \frac{\partial(\mathcal{L}_{tot})}{\partial \theta_{st}}, \\ \theta_{te} \leftarrow \alpha \theta_{te} + (1 - \alpha) \theta_{st}, \end{cases} \quad (1a)$$

$$(1b)$$

where  $\mathcal{L}_{tot}$  denotes the total loss,  $\eta$  denotes learning rate, and  $\alpha$  denotes EMA coefficient.

### 3.2 Dual-source Enhanced Pseudo-label Fusion

Starting from the mean teacher baseline, a central challenge in SFOD lies in generating reliable pseudo-labels, which directly affect the model’s discriminability. Existing approaches attempt to refine low-confidence predictions or leverage soft-label learning (Yoon et al. 2024; Chen, Wang, and Zhang 2023), but they inherently rely on the biased knowledge of the source model, often leading to overconfident or inaccurate labels. DT (Lavoie, Mahmoud, and Waslander 2025) circumvents this by training a DINOv2-based labeler on source data to generate pseudo-labels for the target domain. However, this violates the core source-free constraint of SFOD and proves ineffective when adapted to noisy target data. To address this, we explore the use of powerful object detection VFMs such as Grounding DINO (Liu et al. 2024), which can act as zero-shot labelers in the target domain. However, while VFMs offer strong generalization, they often underperform under domain shifts (Zhang et al. 2024). Motivated by this, we propose **Dual-source Enhanced Pseudo-label Fusion (DEPF)**, which fuses the generalizable predictions from VFMs with the domain-adapted cues from the

---

**Algorithm 1: DEPF**


---

**Require:** Predictions from two models:  $\mathcal{B}_1, \mathcal{B}_2$ ; IoU threshold  $\beta$   
**Ensure:** Fused predictions  $\mathcal{P}$

- 1: Merge all predictions:  $\mathcal{B} \leftarrow \mathcal{B}_1 \cup \mathcal{B}_2$
- 2: Group  $\mathcal{B}$  into clusters using box IoU  $> \beta$
- 3: **for** all cluster  $\mathcal{C}_m = \{(b_k, p_k)\}_{k=1}^n$  **do**
- 4:   Compute entropy-based weights  $\tilde{\mathbf{w}}_k \propto 1/H(p_k)$
- 5:   Fuse box:  $\hat{b} = \sum_k \tilde{\mathbf{w}}_k b_k$ ; score:  $\hat{p} = \sum_k \tilde{\mathbf{w}}_k p_k$
- 6:   Final label:  $\hat{y} = \arg \max_c \hat{p}^{(c)}$
- 7:   Append  $(\hat{b}, \hat{y})$  to  $\mathcal{P}$
- 8: **end for**
- 9: **return**  $\mathcal{P}$

---

teacher model. This is achieved via an entropy-guided fusion strategy that dynamically balances contributions from both sources to produce more reliable pseudo-labels.

To fuse multi-source bounding boxes, Weighted Box Fusion (WBF) (Solovyev, Wang, and Gabruseva 2021) is a straightforward approach that averages overlapping boxes based on confidence scores. However, WBF introduces two critical issues: (1) it requires tuning a global confidence weight, and (2) it merges boxes by class label. This can lead to errors when different sources assign conflicting labels to the same object, which is a frequent scenario due to differing domain perspectives.

To overcome these limitations, we discard class labels during box clustering and instead group overlapping boxes using a large IoU threshold. This allows us to handle label discrepancies more flexibly. For each cluster of overlapping boxes  $\{(b_k, p_k)\}_{k=1}^n$ , where  $b_k \in \mathbb{R}^4$  denotes the box coordinates and  $p_k \in [0, 1]^C$  the class probability vector, we compute the Shannon entropy  $H(p_k)$  of each prediction. We then assign inverse-entropy weights, giving higher influence to more certain predictions. The final fused box and class probability are computed via a weighted average using these normalized weights. The resulting pseudo-label set  $\mathcal{P} = \{(\hat{b}_i, \hat{y}_i)\}_{i=1}^{n_p}$  is obtained by selecting the class with the highest fused probability for each box. The fusion procedure is outlined in Algorithm 1, while a more detailed version is provided in the Appendix due to limited space. Through this entropy-aware design, our framework integrates predictions from both the teacher and VFM, yielding pseudo-labels that are more robust to label noise and domain shifts, leading to improved discriminability.

### 3.3 Patch-weighted Global Feature Alignment

As previously discussed, both discriminability and transferability are crucial for effective adaptation. While DEPF improves discriminability by enhancing pseudo-label quality, we now focus on boosting transferability through feature alignment. To address this, prior SFOD works have aligned features between teacher and student networks using strategies such as graph-based matching (Li et al. 2022a) or adversarial learning (Chu et al. 2023). However, these methods operate solely within the teacher-student paradigm and thus

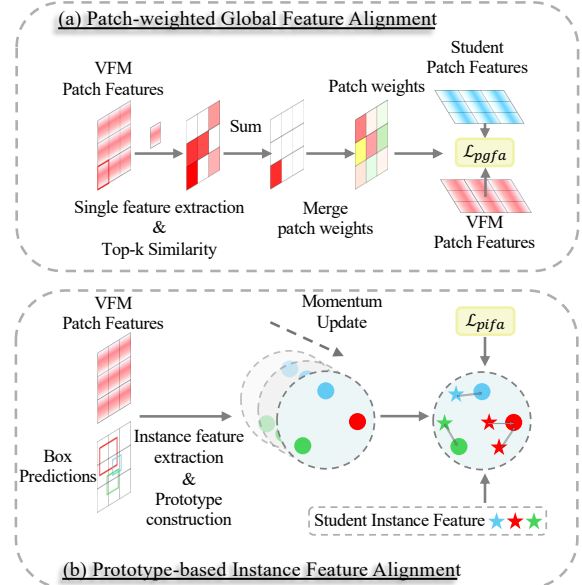


Figure 3: PIFA and PGFA. PGFA adopts similarity-based patch weights for fine-grained global feature fusion. PIFA extracts instance feature from VFM to construct a momentum-updated prototype for contrastive alignment with student instance feature.

inherit source-induced biases and limited decision boundaries. Vision Foundation Models (VFs), particularly DINOv2, offer a broader and more transferable feature space due to large-scale pretraining. DT (Lavoie, Mahmoud, and Waslander 2025) explores feature alignment between a student backbone and a frozen DINOv2 using patch-level cosine similarity. Yet, it assumes equal contribution from all patches, neglecting the varying semantic importance and domain invariance across regions.

To address this, we propose a **Patch-weighted Global Feature Alignment (PGFA)** module that introduces an adaptive patch-wise weighting scheme. We assign a weight to each patch based on its semantic coherence with other patches in the same image. The calculation proceeds in three steps: First, for each image in a minibatch, we compute the pairwise cosine similarity between all its  $L_2$ -normalized DINOv2 patch features ( $\hat{\mathbf{F}}_b^D = \mathbf{F}_b^D / \|\mathbf{F}_b^D\|_2$ , where  $D$  stands for DINOv2 and  $b$  stands for batch index). This results in a similarity matrix  $\mathbf{S}_b \in \mathbb{R}^{N \times N}$ , where  $s_{b,i,j} = \langle \hat{\mathbf{F}}_{b,i}^D, \hat{\mathbf{F}}_{b,j}^D \rangle$  and  $N \times N$  is the number of patches. Second, we apply a temperature-controlled softmax function row-wise to this matrix to obtain a probability distribution for each patch's similarity to all others. This yields a new matrix  $\mathbf{P}_b \in \mathbb{R}^{N \times N}$ :

$$\mathbf{P}_{b,i,j} = \frac{\exp(s_{b,i,j}/\tau)}{\sum_{l=1}^N \exp(s_{b,i,l}/\tau)}, \quad (2)$$

where  $\tau = 0.07$  is a temperature parameter. Finally, the unnormalized weight  $\mathbf{w}_{b,i}$  for patch  $i$  is calculated by summing the probabilities of its top- $k$  most similar patches. Let  $\mathcal{T}_k(i)$  be the set of indices for the top- $k$  values in the  $i$ -th row of

Table 1: Results of cross-weather adaptation (Cityscapes to Foggy Cityscapes).

Method	Source-Free	Detector	Truck	Car	Rider	Person	Train	Motor	Bicycle	Bus	mAP
Source	-	DETR	15.1	46.5	39.3	38.9	4.0	21.8	36.8	34.2	29.6
CAT (Kennerley et al. 2024)	✗	Faster R-CNN	40.8	63.7	57.1	44.6	49.7	44.9	53.0	66.0	52.5
DT (Lavoie, Mahmoud, and Waslander 2025)	✗		47.2	65.4	60.0	48.5	52.9	46.2	56.7	66.5	55.4
MTTrans (Yu et al. 2022)	✗	DETR	25.8	65.2	49.9	47.7	33.9	32.6	46.5	45.9	43.4
BiADT (He et al. 2023)	✗		31.7	69.2	58.9	52.2	45.1	42.6	51.3	55.0	50.8
ACCT (Zeng, Ding, and Lu 2024)	✗		31.1	69.4	58.9	53.6	33.7	42.6	54.4	53.5	49.6
IRG-SFDA (VS, Oza, and Patel 2023)	✓	Faster R-CNN	24.4	51.9	45.2	37.4	25.2	31.5	41.6	39.6	37.1
AASFOD (Chu et al. 2023)	✓		28.1	44.6	44.1	32.3	29.0	31.8	38.9	34.3	35.4
BT (Deng, Li, and Duan 2024)	✓		24.3	52.7	47.1	38.4	36.3	30.2	40.1	44.6	39.2
Simple-SFOD <sup>†</sup> (Hao, Forest, and Fink 2024)	✓		30.2	54.8	44.6	36.5	31.8	29.5	41.0	45.3	39.2
LPLD (Yoon et al. 2024)	✓		29.6	56.6	49.1	39.7	26.4	36.1	43.6	46.3	40.9
DRU (Khanh et al. 2024)	✓	DETR	26.2	62.5	51.5	48.3	34.1	34.2	48.6	43.2	43.6
<b>Ours</b>	✓		36.6	62.8	51.0	48.8	39.9	36.4	48.2	52.7	47.1
Oracle	-	DETR	31.3	71.8	52.9	52.9	41.0	41.4	44.0	53.9	48.7

<sup>†</sup> We report results without BN in the backbone following all other approaches for fair comparison.

$\mathbf{P}_b$ . The weight  $\mathbf{w}_{b,i} = \sum_{j \in \mathcal{T}_k(i)} p_{b,ij}$  is then normalized across all patches for each image:

$$\tilde{\mathbf{w}}_{b,i} = \frac{\mathbf{w}_{b,i}}{\sum_{j=1}^N \mathbf{w}_{b,j} + \varepsilon}, \quad i = 1, \dots, N, \quad (3)$$

where  $N$  is the number of patches and  $\varepsilon$  ensures numerical stability. This process assigns higher weights to salient, semantically consistent patches, while down-weighting noisy or domain-specific regions. For alignment, following DT, we adopt a weighted cosine loss between  $L_2$ -normalized patch features from DINOv2 ( $\mathbf{F}^D$ ) and the student model ( $\mathbf{F}^S$ ):

$$\mathcal{L}_{\text{pgfa}} = \frac{1}{B} \sum_{b=1}^B \sum_{i=1}^N \tilde{\mathbf{w}}_{b,i} (1 - \cos(\mathbf{F}_{b,i}^D, \mathbf{F}_{b,i}^S)), \quad (4)$$

where  $B$  is the batch size. Note that in our implementation, we first input student model patch features into a lightweight alignment module *e.g.* MLP. This loss encourages the student to align more strongly with transferable regions in the VFM feature space, improving global feature transferability in a fine-grained manner.

### 3.4 Prototype-based Instance Feature Alignment

While PGFA enhances transferability by aligning global features, accurate object detection further relies on instance-level representations. Given the rich semantic priors in VFM, we propose leveraging them also as semantic anchors to guide instance recognition and complement global alignment. Specifically, we design **Prototype-based Instance Feature Alignment (PIFA)**, which constructs class-wise prototypes from VFM features and applies prototype-based contrastive learning to enforce semantic consistency, facilitating more robust instance-level alignment.

**Prototype update.** We first extract a global feature map  $\mathbf{F}^D \in \mathbb{R}^{C \times H \times W}$  from the VFM backbone. Given pseudo-labeled boxes  $(b_{k'}, y_{k'})_{k'=1}^{n'}$ , we apply RoIAlign (He et al.

2017) to obtain instance features:

$$\mathbf{f}_c^t = \frac{1}{N_c} \sum_{y_{k'}=c} \text{RoIAlign}(\mathbf{F}^D, b_{k'}), \quad (5)$$

where  $\mathbf{f}_c^t$  is the mean feature for class  $c$  in the current batch.

Inspired by momentum prototype (Li, Xiong, and Hoi 2020), to maintain stable and evolving class-level semantics, we update the prototype  $\mathbf{p}_c^t$  using EMA:

$$\mathbf{p}_c^t = \mu \mathbf{p}_c^{t-1} + (1 - \mu) \mathbf{f}_c^t, \quad (6)$$

where  $\mu = 0.999$  following previous approaches (Li, Xiong, and Hoi 2020). This momentum update smooths temporal fluctuations in the class-wise feature representation while gradually incorporating new semantic information.

**Contrastive learning.** To align the feature spaces of the VFM and the student model’s instance features, we first pass the patch-level features from the student model through a lightweight alignment module (*e.g.*, an MLP). After projection, both the resulting features  $\mathbf{f}_i$  and the prototypes  $\mathbf{p}_c$  are  $L_2$ -normalized to ensure consistent feature magnitudes and facilitate effective similarity computation. Given pseudo label  $\hat{y}_i$  obtained in DEPF, the contrastive loss is computed using InfoNCE (Oord, Li, and Vinyals 2018):

$$\mathcal{L}_{\text{pifa}} = -\frac{1}{M} \sum_{i=1}^M \log \frac{\exp(\mathbf{f}_i^\top \mathbf{p}_{\hat{y}_i} / \tau)}{\sum_{c=1}^K \exp(\mathbf{f}_i^\top \mathbf{p}_c / \tau)}, \quad (7)$$

where  $\tau$  is a temperature hyperparameter and  $M$  is the number of non-empty prototypes. This loss encourages each instance-level feature to align closely with its corresponding class prototype while being repelled from other class prototypes. The use of VFM-guided prototypes as anchors ensures that the student model learns instance features that are semantically aligned and more domain-invariant, leading to improved instance-level feature transferability and class-wise discriminability.

Table 2: Results on cross-scene adaptation (Cityscapes to BDD100K). “FRCNN” stands for Faster R-CNN

Method	SF	Detector	Truck	Car	Rider	Prsn	Bike	Motor	Bus	mAP
Source	-	DETR	17.5	57.0	29.4	43.7	15.6	17.7	17.6	28.3
AASFOD (Chu et al. 2023)	✓	FRCNN	26.6	50.2	36.3	33.2	22.5	28.2	24.4	31.6
BT (Deng, Li, and Duan 2024)	✓		24.2	50.4	34.6	32.7	28.5	24.7	24.9	31.4
DRU (Khanh et al. 2024)	✓	DETR	27.1	62.7	36.9	45.8	32.5	22.7	28.1	36.6
<b>Ours</b>	✓	DETR	33.2	72.3	44.2	54.9	29.0	32.9	34.8	43.0
Oracle	-	DETR	66.9	87.9	56.4	74.9	53.8	68.3	55.0	66.2

Table 3: Results of synthetic-to-real (Sim10k to Cityscapes, S2R) and cross-scene (KITTI to Cityscapes, K2C) adaptation. We report car AP@50 for each method under each scenario.

Method	Source-Free	Detector	mAP	
			S2R	K2C
Source	-	DETR	50.8	33.9
SFA (Wang et al. 2021)	✗	DETR	52.6	46.7
DA-DETR (Zhang et al. 2023)	✗	DETR	54.7	48.9
IRG-SFDA (VS, Oza, and Patel 2023)	✓	Faster R-CNN	46.9	45.2
AASFOD (Chu et al. 2023)	✓		44.9	44.0
SF-UT (Hao, Forest, and Fink 2024)	✓		55.4	46.2
LPLD (Yoon et al. 2024)	✓		49.4	51.3
DRU (Khanh et al. 2024)	✓	DETR	58.7	45.1
<b>Ours</b>	✓	DETR	67.4	54.7
Oracle	-	DETR	75.9	75.9

### 3.5 Overall Objective

For model optimization, the student is optimized to minimize the weighted summation of the original detection loss  $\mathcal{L}_{\text{det}}$  calculated with pseudo labels, and the proposed  $\mathcal{L}_{\text{pgfa}}$  and  $\mathcal{L}_{\text{pifa}}$  losses:

$$\mathcal{L}_{\text{tot}} = \mathcal{L}_{\text{det}} + \lambda(\mathcal{L}_{\text{pgfa}} + \mathcal{L}_{\text{pifa}}). \quad (8)$$

The teacher model is then updated through an exponential moving average of student parameters as stated in Eq. 1b.

## 4 Experiments

### 4.1 Datasets and Settings

We evaluate our method on six widely-used object detection datasets: Cityscapes, Foggy Cityscapes, Sim10k, KITTI, BDD100K, and ACDC. We conclude the settings into three domain adaptation scenarios: cross-weather, synthetic-to-real, and cross-scene.

**Cross-weather Adaptation.** Cityscapes (Cordts et al. 2016) contains 2,975 training and 500 validation images of urban scenes. Its synthetic variant, Foggy Cityscapes (Sakaridis, Dai, and Van Gool 2018), overlays fog at varying densities; we follow prior work and adopt the 0.02 fog level. Additionally, ACDC (Sakaridis, Dai, and Van Gool 2021) includes four challenging conditions (snow, rain, night, and fog) to further evaluate robustness under diverse weather.

**Synthetic-to-Real Adaptation.** Sim10k (Johnson-Roberson et al. 2017), generated from the GTA V engine, provides 9,000 training and 1,000 validation images and serves as the synthetic source. We use Cityscapes as the real-world target to assess synthetic to real generalization.

Table 4: Ablation study on component analysis. Mean Teacher baseline is reproduced with our hyperparameter setting for fair comparison.

Mean Teacher (Tavainen and Valpola 2017)	PGFA	PIFA	DEPF	mAP / Gain
✓				42.3 / -
✓	✓			43.4 / +1.1
✓		✓		43.9 / +1.6
✓	✓	✓		45.0 / +2.7
✓			✓	45.9 / +3.6
✓	✓		✓	46.3 / +4.0
✓		✓	✓	46.5 / +4.2
✓	✓	✓	✓	✓ (w/o $\bar{w}_b$ )
✓	✓	✓	✓	46.8 / +4.5
✓		✓	✓	46.5 / +4.2
✓	✓	✓	✓	47.1 / +4.8

**Cross-scene Adaptation.** We consider two cross-scene transfers: First, following prior work, we transfer from Cityscapes to the daytime split of BDD100K (Yu et al. 2020) (36,728 training and 5,258 validation images). Second, we transfer from KITTI (Geiger, Lenz, and Urtasun 2012) (7,481 labeled images) to Cityscapes. These two settings test the model’s ability to adapt across cities, camera perspectives, and environmental variations.

### 4.2 Implementation Details

We set  $\mu = 0.9$  in Eq. 6 and  $\lambda = 1$  in Eq. 8.  $\alpha$  in Eq. 1b is set to 0.999 with EMA applied every 5 iterations. We train for 30 epochs with a learning rate of  $5 \times 10^{-5}$  and batch size of 8. See Appendix for more details.

### 4.3 Comparisons with State-of-the-art

We evaluate our method under various SFOD scenarios using Deformable DETR as the base detector. In the cross-weather setting, our approach achieves 47.1% mAP, surpassing DRU (Khanh et al. 2024) (43.6%) and LPLD (Yoon et al. 2024) (40.9%), with especially large gains in challenging classes such as Truck (+10.4%) and Bus (+9.5%). On the Cityscapes-to-ACDC benchmark, our method consistently outperforms all baselines across all weather conditions. For cross-scene adaptation, we achieve a 6.4% mAP gain over DRU on Cityscapes-to-BDD100K, effectively leveraging the large-scale unlabeled target data. Our performance is also competitive with the non-source-free DT (Lavoie, Mahmoud, and Waslander 2025), trailing by only 4.8% despite not using source data. On Cityscapes-to-KITTI, we outperform all prior SFOD and DAOD methods by a notable margin. In the Sim10k-to-Cityscapes (synthetic-to-real) setting, our method improves car AP by 8.5% over DRU and 12.7% over DA-DETR, demonstrating strong domain adaptation capability across diverse settings.

### 4.4 Ablation Study

We conduct ablation experiments are conducted on the Cityscapes-to-Foggy Cityscapes setting, consistent with the main experiments.

**Component Effectiveness.** We evaluate each proposed module, including PGFA, PIFA, and DEPF. As shown in Tab. 4, each component brings noticeable gains over the Mean Teacher (MT) baseline, and their combination leads

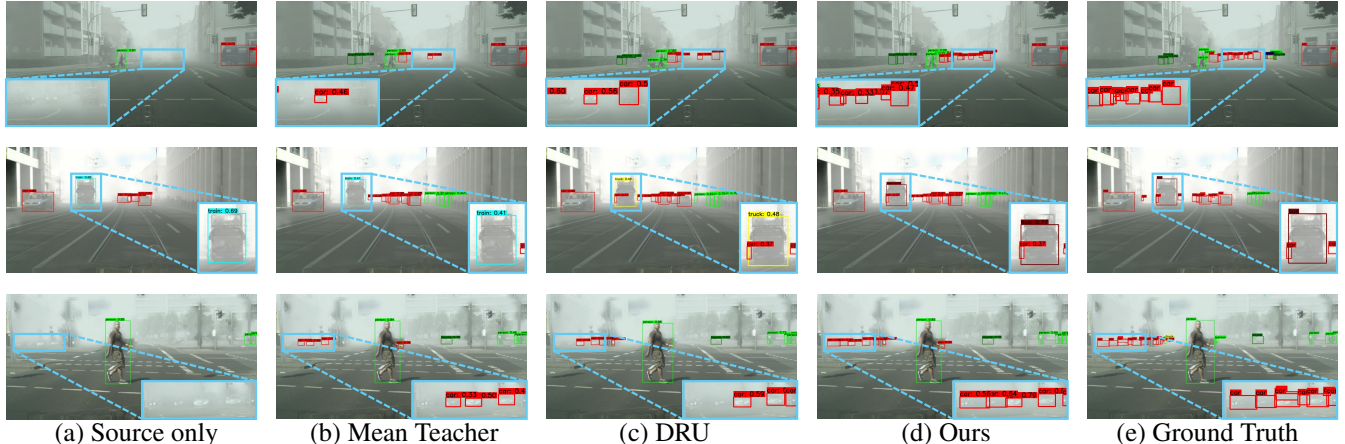


Figure 4: Detection visualization on the Cityscapes-to-Foggy Cityscapes adaptation scenario among (a) Source only, (b) Mean Teacher, (c) DRU, (d) Ours, (e) Ground Truth. We zoom in the discriminative regions for each set of predictions.

Table 5: Results of cross-weather adaptation (Cityscapes-to-ACDC) on Snow, Rain, Night, Fog. “FRCNN” stands for Faster R-CNN. “SF” stands for Source-free. We report mAP@50 for each method under each scenario.

Method	SF	Detector	Snow	Rain	Night	Fog
AT (Li et al. 2022b)	✗	FRCNN	55.2	37.7	29.5	62.2
DT (Lavoie, Mahmoud, and Waslander 2025)	✗		56.8	39.0	36.4	68.6
DRU (Khanh et al. 2024)	✓	DETR	37.9	26.3	16.5	45.4
<b>Ours</b>	✓		<b>47.9</b>	<b>32.1</b>	<b>23.0</b>	<b>54.0</b>

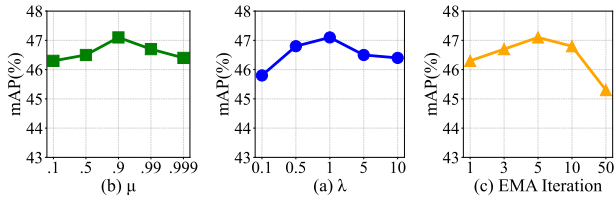


Figure 5: Hyperparameter sensitivity.  $\mu$  is the momentum for prototype update,  $\lambda$  is the loss balancing factor, EMA iteration is the number of iterations for every EMA update.

to 47.1% mAP, a 4.8% improvement over MT. This confirms their complementary roles in improving transferability and discriminability. Additionally, we assess the effect of the proposed weights: patch-wise distillation weight  $\tilde{w}_b$  in PGFA and label fusion weight  $\tilde{w}_k$  in DEPF. Including these weights yields further gains of 0.6% and 0.3% mAP, respectively, highlighting the importance of emphasizing informative regions and predictions.

**Hyperparameter Sensitivity.** We evaluate three key hyperparameters: prototype momentum  $\mu$  (Eq. 6), loss balancing factor  $\lambda$  (Eq. 8), and the EMA update interval, *i.e.*, the number of iterations between teacher updates. As shown in Fig. 5, our method remains robust across a broad range of settings. However, updating prototypes too frequently or too rarely degrades performance due to pseudo-label noise. An EMA interval of 5 yields the best results, balancing stabil-

ity and timely adaptation, consistent with prior studies (Chu et al. 2023; Zhao et al. 2024a).

#### 4.5 Visualization

To qualitatively assess the effectiveness of our approach, we conduct visualization experiments on detection results. As shown in Fig. 4, our method demonstrates clear advantages over the baselines. It successfully detects challenging objects and produces correct classifications for visually ambiguous instances (line 2, where *bus* is misclassified as *train* by MT and as *truck* by DRU), highlighting the benefits of our method and the improved optimization enabled by reliable pseudo-labels. We also present pseudo-label visualizations in the Appendix.

#### 4.6 Additional Experiments

Additional experiments, such as detector variants, zero-shot Grounding DINO performance, efficiency analysis, etc., are provided in the Appendix due to space limitations.

### 5 Conclusion

This paper explores an under-investigated direction of enhancing Source-Free Object Detection (SFOD) using Vision Foundation Models (VFs) to improve both discriminability and transferability in self-training pipelines. We introduce a simple yet effective framework consisting of three modules: PGFA, PIFA, and DEPF, each focusing on global feature alignment, instance-level feature alignment, and pseudo-label refinement, respectively. By effectively integrating generic knowledge from VFs, our framework achieves consistent improvements in SFOD performance, as validated by extensive experiments. These results indicate that integrating VFs into more scalable and robust DAOD and SFOD frameworks is a promising direction for future research. In future work, we aim to explore more about richer vision-language multimodal feature spaces to enhance alignment effectiveness and to incorporate VFs into more challenging cross-domain object detection scenarios.

## Acknowledgments

This work was supported in part by the National Key R&D Program of China (Grant No.2023YFF0725001), in part by the National Natural Science Foundation of China (Grant No.92370204), in part by the Guangdong Basic and Applied Basic Research Foundation (Grant No.2023B1515120057), in part by the Key-Area Special Project of Guangdong Provincial Ordinary Universities(2024ZDZX1007), in part by the Education Bureau of Guangzhou.

## References

Awais, M.; Naseer, M.; Khan, S.; Anwer, R. M.; Cholakkal, H.; Shah, M.; Yang, M.-H.; and Khan, F. S. 2025. Foundation models defining a new era in vision: a survey and outlook. *IEEE Transactions on Pattern Analysis and Machine Intelligence*.

Chen, M.; Chen, W.; Yang, S.; Song, J.; Wang, X.; Zhang, L.; Yan, Y.; Qi, D.; Zhuang, Y.; Xie, D.; et al. 2022. Learning domain adaptive object detection with probabilistic teacher. *arXiv preprint arXiv:2206.06293*.

Chen, Z.; Wang, Z.; and Zhang, Y. 2023. Exploiting low-confidence pseudo-labels for source-free object detection. In *Proceedings of the 31st ACM International Conference on Multimedia*, 5370–5379.

Chu, Q.; Li, S.; Chen, G.; Li, K.; and Li, X. 2023. Adversarial alignment for source free object detection. In *Proceedings of the AAAI conference on artificial intelligence*, volume 37, 452–460.

Cordts, M.; Omran, M.; Ramos, S.; Rehfeld, T.; Enzweiler, M.; Benenson, R.; Franke, U.; Roth, S.; and Schiele, B. 2016. The cityscapes dataset for semantic urban scene understanding. In *IEEE/CVF Conference on Computer Vision and Pattern Recognition*, 3213–3223.

Deng, J.; Li, W.; and Duan, L. 2024. Balanced teacher for source-free object detection. *IEEE Transactions on Circuits and Systems for Video Technology*, 34(8): 7231–7243.

Dosovitskiy, A.; Beyer, L.; Kolesnikov, A.; Weissenborn, D.; Zhai, X.; Unterthiner, T.; Dehghani, M.; Minderer, M.; Heigold, G.; Gelly, S.; et al. 2020. An image is worth 16x16 words: Transformers for image recognition at scale. *arXiv preprint arXiv:2010.11929*.

Geiger, A.; Lenz, P.; and Urtasun, R. 2012. Are we ready for autonomous driving? the kitti vision benchmark suite. In *2012 IEEE conference on computer vision and pattern recognition*, 3354–3361. IEEE.

Han, J.; Wang, Y.; and Chen, L. 2025. VFM-Guided Semi-Supervised Detection Transformer under Source-Free Constraints for Remote Sensing Object Detection. *arXiv preprint arXiv:2508.11167*.

Hao, Y.; Forest, F.; and Fink, O. 2024. Simplifying source-free domain adaptation for object detection: Effective self-training strategies and performance insights. In *European Conference on Computer Vision*, 196–213. Springer.

He, K.; Gkioxari, G.; Dollár, P.; and Girshick, R. 2017. Mask r-cnn. In *Proceedings of the IEEE international conference on computer vision*, 2961–2969.

He, L.; Wang, W.; Chen, A.; Sun, M.; Kuo, C.-H.; and Todorovic, S. 2023. Bidirectional alignment for domain adaptive detection with transformers. In *IEEE/CVF International Conference on Computer Vision*, 18775–18785.

Jocher, G.; Stoken, A.; Borovec, J.; NanoCode012; ChristopherSTAN; Changyu, L.; Laughing; tkianai; Hogan, A.; lorenzomammama; yxNONG; AlexWang1900; Diaconu, L.; Marc; wanghaoyang0106; ml5ah; Doug; Ingham, F.; Frederik; Guilhen; Hatovix; Poznanski, J.; Fang, J.; Yu, L.; changyu98; Wang, M.; Gupta, N.; Akhtar, O.; PetrDvoracek; and Rai, P. 2020. ultralytics/yolov5: v3.1 - Bug Fixes and Performance Improvements.

Johnson-Roberson, M.; Barto, C.; Mehta, R.; Sridhar, S. N.; Rosaen, K.; and Vasudevan, R. 2017. Driving in the matrix: Can virtual worlds replace human-generated annotations for real world tasks? In *IEEE International Conference on Robotics and Automation*, 746–753.

Kennerley, M.; Wang, J.-G.; Veeravalli, B.; and Tan, R. T. 2024. Cat: Exploiting inter-class dynamics for domain adaptive object detection. In *Proceedings of the IEEE/CVF Conference on Computer Vision and Pattern Recognition*, 16541–16550.

Khanh, T. L. B.; Nguyen, H.-H.; Pham, L. H.; Tran, D. N.-N.; and Jeon, J. W. 2024. Dynamic retraining-updating mean teacher for source-free object detection. In *European Conference on Computer Vision*, 328–344. Springer.

Kirillov, A.; Mintun, E.; Ravi, N.; Mao, H.; Rolland, C.; Gustafson, L.; Xiao, T.; Whitehead, S.; Berg, A. C.; Lo, W.-Y.; et al. 2023. Segment anything. In *Proceedings of the IEEE/CVF international conference on computer vision*, 4015–4026.

Kundu, J. N.; Kulkarni, A. R.; Bhambri, S.; Mehta, D.; Kulkarni, S. A.; Jampani, V.; and Radhakrishnan, V. B. 2022. Balancing discriminability and transferability for source-free domain adaptation. In *International conference on machine learning*, 11710–11728. PMLR.

Lavoie, M.-A.; Mahmoud, A.; and Waslander, S. L. 2025. Large Self-Supervised Models Bridge the Gap in Domain Adaptive Object Detection. In *Proceedings of the Computer Vision and Pattern Recognition Conference*, 4692–4702.

Li, H.; Zhang, R.; Yao, H.; Song, X.; Hao, Y.; Zhao, Y.; Li, L.; and Chen, Y. 2023a. Learning domain-aware detection head with prompt tuning. *Advances in Neural Information Processing Systems*, 36: 4248–4262.

Li, J.; Xiong, C.; and Hoi, S. C. 2020. Mopro: Webly supervised learning with momentum prototypes. *arXiv preprint arXiv:2009.07995*.

Li, J.; Yu, Z.; Du, Z.; Zhu, L.; and Shen, H. T. 2024a. A comprehensive survey on source-free domain adaptation. *IEEE Transactions on Pattern Analysis and Machine Intelligence*, 46(8): 5743–5762.

Li, P.; He, Y.; Yu, F. R.; Song, P.; Yin, D.; and Zhou, G. 2023b. IGG: Improved graph generation for domain adaptive object detection. In *Proceedings of the 31st ACM international conference on multimedia*, 1314–1324.

Li, S.; Ye, M.; Zhou, L.; Li, N.; Xiao, S.; Tang, S.; and Zhu, X. 2024b. Cloud object detector adaptation by integrating

different source knowledge. *Advances in Neural Information Processing Systems*, 37: 25251–25283.

Li, S.; Ye, M.; Zhu, X.; Zhou, L.; and Xiong, L. 2022a. Source-free object detection by learning to overlook domain style. In *Proceedings of the IEEE/CVF conference on computer vision and pattern recognition*, 8014–8023.

Li, W.; Liu, X.; and Yuan, Y. 2022. Sigma: Semantic-complete graph matching for domain adaptive object detection. In *Proceedings of the IEEE/CVF conference on computer vision and pattern recognition*, 5291–5300.

Li, X.; Chen, W.; Xie, D.; Yang, S.; Yuan, P.; Pu, S.; and Zhuang, Y. 2021. A free lunch for unsupervised domain adaptive object detection without source data. In *Proceedings of the AAAI Conference on Artificial Intelligence*, volume 35, 8474–8481.

Li, Y.-J.; Dai, X.; Ma, C.-Y.; Liu, Y.-C.; Chen, K.; Wu, B.; He, Z.; Kitani, K.; and Vajda, P. 2022b. Cross-domain adaptive teacher for object detection. In *Proceedings of the IEEE/CVF conference on computer vision and pattern recognition*, 7581–7590.

Liu, F.; Zhang, X.; Wan, F.; Ji, X.; and Ye, Q. 2021a. Domain contrast for domain adaptive object detection. *IEEE Transactions on Circuits and Systems for Video Technology*, 32(12): 8227–8237.

Liu, S.; Zeng, Z.; Ren, T.; Li, F.; Zhang, H.; Yang, J.; Jiang, Q.; Li, C.; Yang, J.; Su, H.; et al. 2024. Grounding dino: Marrying dino with grounded pre-training for open-set object detection. In *European conference on computer vision*, 38–55. Springer.

Liu, Z.; Lin, Y.; Cao, Y.; Hu, H.; Wei, Y.; Zhang, Z.; Lin, S.; and Guo, B. 2021b. Swin transformer: Hierarchical vision transformer using shifted windows. In *Proceedings of the IEEE/CVF international conference on computer vision*, 10012–10022.

Lu, S.; Chen, Y.; Feng, W.; Fan, J.; Li, F.; Zhang, Z.; Lv, J.; Shen, J.; Law, C.; and Liang, J. 2025a. Uni-layout: Integrating human feedback in unified layout generation and evaluation. In *Proceedings of the 33rd ACM International Conference on Multimedia*, 7709–7718.

Lu, S.; Wang, Y.; Sheng, L.; He, L.; Zheng, A.; and Liang, J. 2025b. Out-of-distribution detection: A task-oriented survey of recent advances. *ACM Computing Surveys*, 58(2): 1–39.

Maaten, L. v. d.; and Hinton, G. 2008. Visualizing data using t-SNE. *Journal of machine learning research*, 9(Nov): 2579–2605.

Oord, A. v. d.; Li, Y.; and Vinyals, O. 2018. Representation learning with contrastive predictive coding. *arXiv preprint arXiv:1807.03748*.

Oquab, M.; Dariseti, T.; Moutakanni, T.; Vo, H.; Szafraniec, M.; Khalidov, V.; Fernandez, P.; Haziza, D.; Massa, F.; El-Nouby, A.; et al. 2023. Dinov2: Learning robust visual features without supervision. *arXiv preprint arXiv:2304.07193*.

Paszke, A.; Gross, S.; Massa, F.; Lerer, A.; Bradbury, J.; Chanan, G.; Killeen, T.; Lin, Z.; Gimelshein, N.; Antiga, L.; et al. 2019. Pytorch: An imperative style, high-performance deep learning library. *Advances in neural information processing systems*, 32.

Ren, S.; He, K.; Girshick, R.; and Sun, J. 2016. Faster R-CNN: Towards real-time object detection with region proposal networks. *IEEE transactions on pattern analysis and machine intelligence*, 39(6): 1137–1149.

Sakaridis, C.; Dai, D.; and Van Gool, L. 2018. Semantic foggy scene understanding with synthetic data. *International Journal of Computer Vision*, 126: 973–992.

Sakaridis, C.; Dai, D.; and Van Gool, L. 2021. ACDC: The adverse conditions dataset with correspondences for semantic driving scene understanding. In *Proceedings of the IEEE/CVF international conference on computer vision*, 10765–10775.

Solovyev, R.; Wang, W.; and Gabruseva, T. 2021. Weighted boxes fusion: Ensembling boxes from different object detection models. *Image and Vision Computing*, 107: 104117.

Tarvainen, A.; and Valpola, H. 2017. Mean teachers are better role models: Weight-averaged consistency targets improve semi-supervised deep learning results. *Advances in neural information processing systems*, 30.

Varailhon, S.; Aminbeidokhti, M.; Pedersoli, M.; and Granger, E. 2024. Source-free domain adaptation for yolo object detection. In *European Conference on Computer Vision*, 218–235. Springer.

VS, V.; Oza, P.; and Patel, V. M. 2023. Instance relation graph guided source-free domain adaptive object detection. In *Proceedings of the IEEE/CVF conference on computer vision and pattern recognition*, 3520–3530.

Wang, F.; and Liu, H. 2021. Understanding the behaviour of contrastive loss. In *Proceedings of the IEEE/CVF conference on computer vision and pattern recognition*, 2495–2504.

Wang, W.; Cao, Y.; Zhang, J.; He, F.; Zha, Z.-J.; Wen, Y.; and Tao, D. 2021. Exploring sequence feature alignment for domain adaptive detection transformers. In *ACM International Conference on Multimedia*, 1730–1738.

Wang, Y.; Huang, T.; He, C.; Li, Q.; and Gao, J. 2025. Simple and Efficient Heterogeneous Temporal Graph Neural Network. *arXiv preprint arXiv:2510.18467*.

Weng, W.; and Yuan, C. 2024. Mean Teacher DETR with Masked Feature Alignment: A Robust Domain Adaptive Detection Transformer Framework. In *AAAI Conference on Artificial Intelligence*, volume 38, 5912–5920.

Wu, J.; Feng, M.; Zhang, S.; Jin, R.; Che, F.; Wen, Z.; and Tao, J. 2025. Boosting multimodal reasoning with mcts-automated structured thinking. *arXiv e-prints*, arXiv-2502.

Yang, L.; Kang, B.; Huang, Z.; Xu, X.; Feng, J.; and Zhao, H. 2024. Depth anything: Unleashing the power of large-scale unlabeled data. In *Proceedings of the IEEE/CVF conference on computer vision and pattern recognition*, 10371–10381.

Yao, H.; Zhao, S.; Lu, S.; Chen, H.; Li, Y.; Liu, G.; Xing, T.; Yan, C.; Tao, J.; and Ding, G. 2025. Source-Free Object Detection With Detection Transformer. *IEEE Transactions on Image Processing*, 34: 5948–5963.

Yao, X.; Zhao, S.; Xu, P.; and Yang, J. 2021. Multi-source domain adaptation for object detection. In *Proceedings of*

the IEEE/CVF international conference on computer vision, 3273–3282.

Yoon, I.; Kwon, H.; Kim, J.; Park, J.; Jang, H.; and Sohn, K. 2024. Enhancing source-free domain adaptive object detection with low-confidence pseudo label distillation. In *European Conference on Computer Vision*, 337–353. Springer.

Yu, F.; Chen, H.; Wang, X.; Xian, W.; Chen, Y.; Liu, F.; Madhavan, V.; and Darrell, T. 2020. BDD100K: A Diverse Driving Dataset for Heterogeneous Multitask Learning. In *IEEE/CVF Conference on Computer Vision and Pattern Recognition*, 2633–2642.

Yu, J.; Liu, J.; Wei, X.; Zhou, H.; Nakata, Y.; Gudovskiy, D.; Okuno, T.; Li, J.; Keutzer, K.; and Zhang, S. 2022. MTTrans: Cross-domain object detection with mean teacher transformer. In *European Conference on Computer Vision*, 629–645. Springer.

Zeng, Z.; Ding, Y.; and Lu, H. 2024. Enhancing cross-domain detection: adaptive class-aware contrastive transformer. In *IEEE International Conference on Acoustics, Speech and Signal Processing*, 6670–6674.

Zhang, H.; Su, Y.; Xu, X.; and Jia, K. 2024. Improving the generalization of segmentation foundation model under distribution shift via weakly supervised adaptation. In *Proceedings of the IEEE/CVF Conference on Computer Vision and Pattern Recognition*, 23385–23395.

Zhang, J.; Huang, J.; Luo, Z.; Zhang, G.; Zhang, X.; and Lu, S. 2023. Da-detr: Domain adaptive detection transformer with information fusion. In *IEEE/CVF Conference on Computer Vision and Pattern Recognition*, 23787–23798.

Zhang, S.; Zhang, L.; and Liu, Z. 2023. Refined pseudo labeling for source-free domain adaptive object detection. In *ICASSP 2023-2023 IEEE International Conference on Acoustics, Speech and Signal Processing (ICASSP)*, 1–5. IEEE.

Zhao, S.; Hong, X.; Yang, J.; Zhao, Y.; and Ding, G. 2023. Toward Label-Efficient Emotion and Sentiment Analysis. *Proceedings of the IEEE*, 111(10): 1159–1197.

Zhao, S.; Yao, H.; Lin, C.; Gao, Y.; and Ding, G. 2024a. Multi-source-free domain adaptive object detection. *International Journal of Computer Vision*, 132(12): 5950–5982.

Zhao, Y.; Lv, W.; Xu, S.; Wei, J.; Wang, G.; Dang, Q.; Liu, Y.; and Chen, J. 2024b. Detrs beat yolos on real-time object detection. In *Proceedings of the IEEE/CVF conference on computer vision and pattern recognition*, 16965–16974.

Zhu, X.; Su, W.; Lu, L.; Li, B.; Wang, X.; and Dai, J. 2020. Deformable detr: Deformable transformers for end-to-end object detection. *arXiv preprint arXiv:2010.04159*.

## A Detailed Algorithm for DEPF

Here we provide the detailed algorithm for DEPF (Dual-source Enhanced Pseudo-label Fusion), as shown in Algorithm 2.

## B Implementation Details

In this section, we provide the complete implementation details of our method.

For the source model pretraining stage, we train for 40 epochs with a learning rate of  $2 \times 10^{-4}$ , followed by another 10 epochs with a reduced learning rate of  $2 \times 10^{-5}$ . During the target adaptation stage, we set the total batch size to 8 and use a learning rate of  $5 \times 10^{-5}$ . We set the EMA decay factor  $\alpha$  to 0.999 and perform the teacher model update every 5 iterations, ensuring stable updates as suggested by prior works (Chu et al. 2023; Zhao et al. 2024a). For other hyperparameters, we adopt the default settings discussed in the main paper. Specifically, we set  $\mu = 0.9$  as the momentum coefficient in prototype updates, and  $\lambda = 1$  as the balancing weight in the overall objective. For the DEPF module, we set the IoU threshold  $\beta = 0.7$  to cluster and fuse overlapping bounding boxes. In PGFA, we select the top 50 patches with the highest similarity scores to construct patch-wise weights. Both student and VFM features are extracted using  $16 \times 16$  patch tokens. For RoIAlign (He et al. 2017), we fix the output resolution to  $7 \times 7$ , consistent with most standard implementations. We use a temperature parameter of  $\tau = 0.07$  for the contrastive loss in PIFA, following prior practices (Wang and Liu 2021). The lightweight projection heads used in both PGFA and PIFA are three-layer MLPs with a hidden dimension of 512. The input and output dimensions are determined by the channel dimensions of the student detector, student backbone, and visual foundation models.

Our framework is implemented using PyTorch (Paszke et al. 2019). All experiments are conducted on a machine with 4 NVIDIA RTX A6000 GPUs running Ubuntu 22.04 as the operating system.

## C Full Experimental Results

In the main paper, we only report partial results for two adaptation scenarios including (1) Cityscapes-to-BDD100K and (2) Cityscapes-to-ACDC, due to space limitations. Here, we provide the complete results for both settings.

### C.1 Cityscapes-to-BDD100K

For the Cityscapes-to-BDD100K scenario, we include a more comprehensive comparison with additional baseline methods and experimental settings, as shown in Tab. 6. The results demonstrate that our approach consistently surpasses most existing DAOD and source-free object detection (SFOD) methods by a substantial margin—for instance, achieving 6.4% higher mAP than DRU (Khanh et al. 2024) and 4.0% higher than ACCT (Zeng, Ding, and Lu 2024). While our method performs slightly worse than DT (Lavoie, Mahmoud, and Waslander 2025), it is important to note that DT assumes access to both source images and labels, making its setting less constrained than ours. Since DT also

---

### Algorithm 2: DEPF

---

**Require:** Two sets of predictions  $\mathcal{B}_1 = \{(b_i, p_i)\}$ ,  $\mathcal{B}_2 = \{(b_j, p_j)\}$ ; IoU threshold  $\beta$ ; small constant  $\varepsilon$

**Ensure:** Fused pseudo labels  $\{(\hat{b}_{k'}, \hat{y}_{k'})\}$

- 1: Merge predictions:  $\mathcal{B} \leftarrow \mathcal{B}_1 \cup \mathcal{B}_2$
- 2: Initialize empty cluster list:  $\mathcal{C} \leftarrow []$
- 3: **for all**  $(b_k, p_k) \in \mathcal{B}$  **do**
- 4:     Find cluster  $\mathcal{C}_m$  such that  $\exists (b_j, \cdot) \in \mathcal{C}_m$  with  $\text{IoU}(b_k, b_j) > \beta$
- 5:     **if** such cluster exists **then**
- 6:         Add  $(b_k, p_k)$  to cluster  $\mathcal{C}_m$
- 7:     **else**
- 8:         Create new cluster  $\mathcal{C}_{\text{new}} \leftarrow \{(b_k, p_k)\}$  and add to  $\mathcal{C}$
- 9:     **end if**
- 10: **end for**
- 11: Initialize fused label list:  $\mathcal{P} \leftarrow []$
- 12: **for all** cluster  $\mathcal{C}_m = \{(b_k, p_k)\}_{k=1}^n$  **do**
- 13:     **for**  $k = 1$  to  $n$  **do**
- 14:          $H(p_k) \leftarrow -\sum_c p_k^{(c)} \log(p_k^{(c)}) + \varepsilon$
- 15:          $\mathbf{w}_k \leftarrow \frac{1}{H(p_k) + \varepsilon}$
- 16:     **end for**
- 17:     Normalize weights:  $\tilde{\mathbf{w}}_k \leftarrow \text{Norm}(\mathbf{w}_k)$
- 18:     Fuse box:  $\hat{b} \leftarrow \sum_{k=1}^n \tilde{\mathbf{w}}_k b_k$
- 19:     Fuse score:  $\hat{p} \leftarrow \sum_{k=1}^n \tilde{\mathbf{w}}_k p_k$
- 20:     Final label:  $\hat{y} \leftarrow \arg \max_c \hat{p}^{(c)}$
- 21:     Append  $(\hat{b}, \hat{y})$  to  $\mathcal{P}$
- 22: **end for**
- 23: **return**  $\mathcal{P}$

---

incorporates Vision Foundation Models (VFs), its strong performance further highlights the potential of VFs for enhancing cross-domain generalization.

### C.2 Cityscapes-to-ACDC

For the Cityscapes-to-ACDC setting, we report detailed class-wise AP and overall mAP for both DRU (Khanh et al. 2024) and our method, based on our own reproduction and implementation (Tab. 9). The results clearly show that our method consistently outperforms DRU across most categories, further validating the robustness and effectiveness of our approach.

## D Additional Experiments

### D.1 Effectiveness across Backbone Variants

We further evaluate the method across different detector backbones beyond ResNet-50, including Swin Transformer (Liu et al. 2021b) with sizes T(tiny), S(small), B(base), and L(large) and Vision Transformer ViT-B (Dosovitskiy et al. 2020). We give the full results, including per-class AP and mAP. Results in Tab. 8 show consistent gains across all backbones, verifying the robustness of our method across different backbones. These gains demonstrate that our approach not only scales well with model capacity but also complements different feature extraction paradigms, whether convolution-based (ResNet), hierarchical transformer-based (Swin), or pure transformer-based

Table 6: Results on cross-scene adaptation (Cityscapes to BDD100K).

Method	Source-Free	Detector	Truck	Car	Rider	Person	Bicycle	Motor	Bus	mAP
Source	-	DETR	17.5	57.0	29.4	43.7	15.6	17.7	17.6	28.3
CAT (Kennerley et al. 2024)	✗	Faster R-CNN	31.4	61.2	41.5	44.6	31.7	24.4	34.6	38.5
DT (Lavoie, Mahmoud, and Waslander 2025)	✗		44.3	66.6	47.0	51.6	40.8	38.3	45.9	47.8
SFA (Wang et al. 2021)	✗	DETR	19.1	57.5	27.6	40.2	19.2	15.4	23.4	28.9
MTTrans (Yu et al. 2022)	✗		25.1	61.5	30.1	44.1	23.0	17.7	26.9	32.6
MTM (Weng and Yuan 2024)	✗		23.0	68.8	35.1	53.7	28.0	23.8	28.8	37.3
BiADT (He et al. 2023)	✗		17.4	60.9	34.0	42.1	25.7	18.2	19.5	31.1
ACCT (Zeng, Ding, and Lu 2024)	✗		26.0	61.8	41.4	51.8	36.9	31.7	23.4	39.0
SED (Li et al. 2021)	✓	Faster R-CNN	20.6	50.4	32.6	32.4	25.0	18.9	23.4	29.0
AASFOD (Chu et al. 2023)	✓		26.6	50.2	36.3	33.2	22.5	28.2	24.4	31.6
BT (Deng, Li, and Duan 2024)	✓		24.2	50.4	34.6	32.7	28.5	24.7	24.9	31.4
DRU (Khanh et al. 2024)	✓	DETR	27.1	62.7	36.9	45.8	32.5	22.7	28.1	36.6
<b>Ours</b>	✓		<b>33.2</b>	<b>72.3</b>	<b>44.2</b>	<b>54.9</b>	<b>29.0</b>	<b>32.9</b>	<b>34.8</b>	<b>43.0</b>
Oracle	-	DETR	66.9	87.9	56.4	74.9	53.8	68.3	55.0	66.2

Table 7: Comparison of source-free adaptation across different detectors on Foggy Cityscapes. For each detector group, the best per-category AP is highlighted in bold.

Method	Detector	Truck	Car	Rider	Person	Train	Motor	Bicycle	Bus	mAP
Source <sup>†</sup>		19.8	36.1	38.6	31.2	9.1	21.8	30.4	23.5	26.3
IRG <sup>†</sup> (VS, Oza, and Patel 2023)	Faster R-CNN (Ren et al. 2016)	23.8	51.4	46.5	37.5	30.3	28.7	39.5	39.5	37.1
IRG+Ours		<b>29.0</b>	<b>51.7</b>	<b>48.0</b>	<b>37.6</b>	<b>35.4</b>	<b>32.8</b>	<b>42.7</b>	<b>46.8</b>	<b>40.5</b>
Source		29.9	54.0	46.8	38.7	21.9	29.4	39.3	43.7	38.0
MT (Tervainen and Valpola 2017)	RT DETR (Zhao et al. 2024b)	40.2	71.2	52.0	48.8	47.7	40.8	45.3	61.6	51.0
MT+Ours		<b>43.8</b>	<b>73.9</b>	<b>54.3</b>	<b>51.6</b>	<b>53.7</b>	<b>42.2</b>	<b>48.6</b>	<b>66.3</b>	<b>54.3</b>
Source <sup>†</sup>		25.3	59.9	49.1	48.1	18.8	33.2	41.1	32.8	38.5
SF-YOLO <sup>†</sup> (Varailhon et al. 2024)	YOLOv5 (Jocher et al. 2020)	30.0	<b>62.4</b>	<b>53.1</b>	<b>47.9</b>	34.4	36.9	43.4	41.8	43.7
SF-YOLO+Ours		<b>31.1</b>	62.0	53.0	47.7	<b>45.9</b>	<b>39.9</b>	<b>44.9</b>	<b>44.5</b>	<b>46.1</b>

<sup>†</sup> We reproduce the results based on the corresponding publicly available codebases.

(ViT). Importantly, even with lightweight backbones such as Swin-T, our method maintains strong performance, making it suitable for resource-constrained deployment scenarios as well.

## D.2 Effectiveness across Detector Variants

Although our main experiments are conducted using Deformable DETR (Zhu et al. 2020), our method is designed to be detector-agnostic, meaning it can be readily adapted to other detection architectures. To demonstrate this generality, we implement our method on three representative detector variants: Faster R-CNN (Ren et al. 2016), RT-DETR (Zhao et al. 2024b), and YOLOv5 (Jocher et al. 2020).

For ease of implementation and fair comparison, we build on publicly available open-source baselines: we use the IRG (VS, Oza, and Patel 2023) framework for Faster R-CNN and SF-YOLO (Varailhon et al. 2024) for YOLOv5 (specifically, the YOLOv5l variant). For RT-DETR, we implement a simple Mean Teacher (MT) (Tervainen and Valpola 2017) framework as baseline. To avoid conflicts between components, we make the following adjustments:

- For IRG+ours, we disable the instance relation graph and

the graph-based contrastive loss, as they may interfere with our PIFA module’s instance-level contrastive learning.

- For RT-DETR, which relies on ground-truth labels for query selection during training, we disable this mechanism when generating pseudo-labels from the teacher model. Instead, pseudo-labels are used to guide query selection in the student model during training.

As shown in Tab. 7, our method achieves consistent and significant performance gains across all detector variants: +3.4% mAP on Faster R-CNN, +3.3% on RT-DETR, and +2.4% on YOLOv5l. These results confirm the flexibility and effectiveness of our approach across a range of detection paradigms, underscoring its potential for real-world deployment.

## D.3 Zero-shot Grounding DINO Performance

To provide a more comprehensive comparison, we further evaluate the zero-shot performance of Grounding DINO (Liu et al. 2024) on challenging cross-weather adaptation tasks, including Cityscapes-to-Foggy Cityscapes and

Table 8: Per-category AP results across different methods and backbones on Cityscapes-to-Foggy Cityscapes scenario.

Method	Backbone	Truck	Car	Rider	Person	Train	Motor	Bicycle	Bus	mAP
Grounding DINO (Liu et al. 2024)	Swin-B	32.8	49.7	16.7	33.4	19.4	33.3	42.2	46.5	34.3
Source DRU (Khanh et al. 2024)	ResNet50	15.1	46.5	39.3	38.9	4.0	21.8	36.8	34.2	29.6
		26.2	62.5	<b>51.5</b>	48.3	34.1	34.2	<b>48.6</b>	43.2	43.6
		<b>36.6</b>	<b>62.8</b>	51.0	<b>48.8</b>	<b>39.9</b>	<b>36.4</b>	48.2	<b>52.7</b>	<b>47.1</b>
Source DRU (Khanh et al. 2024)	ViT-B	17.8	46.8	41.3	38.2	3.7	24.2	37.2	30.1	29.9
		22.5	62.6	45.9	44.8	20.9	25.5	41.1	39.2	37.8
		<b>33.7</b>	<b>63.2</b>	<b>52.5</b>	<b>49.9</b>	<b>34.4</b>	<b>37.0</b>	<b>47.8</b>	<b>47.4</b>	<b>45.7</b>
Source DRU (Khanh et al. 2024)	Swin-T	30.0	55.5	48.5	45.0	15.8	35.3	42.6	41.3	39.2
		35.0	<b>66.4</b>	49.7	49.8	30.4	38.1	47.6	46.9	45.5
		<b>40.0</b>	<b>66.4</b>	<b>53.1</b>	<b>51.4</b>	<b>34.4</b>	<b>41.7</b>	<b>50.8</b>	<b>46.8</b>	<b>48.1</b>
Source DRU (Khanh et al. 2024)	Swin-S	29.9	56.2	50.5	45.6	<b>35.9</b>	36.6	42.7	46.6	43.0
		37.8	65.8	53.8	50.8	27.6	41.8	49.2	50.7	47.1
		<b>40.9</b>	<b>66.2</b>	<b>55.3</b>	<b>52.2</b>	31.3	<b>44.1</b>	<b>50.8</b>	<b>54.4</b>	<b>49.4</b>
Source DRU (Khanh et al. 2024)	Swin-B	37.7	62.5	51.3	49.3	39.2	38.6	45.2	46.2	46.2
		39.4	<b>69.2</b>	52.5	51.8	42.1	44.7	50.8	56.4	50.9
		<b>43.4</b>	69.1	<b>55.0</b>	<b>53.8</b>	<b>44.8</b>	<b>44.6</b>	<b>53.1</b>	<b>59.3</b>	<b>52.9</b>
Source DRU (Khanh et al. 2024)	Swin-L	39.4	63.5	49.5	49.2	<b>48.9</b>	41.9	45.6	52.7	48.9
		<b>45.0</b>	68.8	52.9	53.1	47.8	45.2	50.5	56.6	52.5
		44.9	<b>69.2</b>	<b>57.1</b>	<b>55.0</b>	44.1	<b>47.6</b>	<b>53.5</b>	<b>57.9</b>	<b>53.7</b>

Table 9: Detailed results of cross-weather adaptation on Cityscapes-to-ACDC benchmark.

Method	Backbone	Scenario	Truck	Car	Rider	Person	Train	Motor	Bicycle	Bus	mAP
DRU (Khanh et al. 2024)	ResNet50	Snow	44.2	62.2	11.7	37.7	64.5	49.1	26.1	8.0	37.9
		Rain	17.8	59.9	11.8	35.8	27.4	36.7	0.0	21.0	26.3
		Night	18.6	40.7	5.3	24.7	11.4	11.9	3.2	- <sup>†</sup>	16.5
		Fog	23.9	64.6	35.5	50.0	66.3	44.1	44.0	34.5	45.4
Grounding DINO (Liu et al. 2024)	Swin-B	Snow	46.6	78.0	0.0	66.5	68.2	48.7	64.5	36.4	51.1
		Rain	53.0	79.7	5.4	41.9	22.8	41.4	16.8	37.5	37.3
		Night	21.4	61.5	3.1	42.3	46.4	10.3	10.3	- <sup>†</sup>	27.9
		Fog	38.3	84.6	18.8	61.9	66.3	46.2	61.4	71.7	56.2
Ours	ResNet50	Snow	48.8	72.2	51.3	42.6	69.7	55.0	42.1	1.5	47.9
		Rain	27.8	71.4	31.2	39.4	21.0	23.3	9.5	32.8	32.1
		Night	14.3	55.0	18.3	33.6	17.3	11.5	11.0	- <sup>†</sup>	23.0
		Fog	35.6	80.3	52.0	55.4	66.3	36.6	40.0	65.6	50.6
Ours	Swin-B	Snow	58.0	73.6	51.1	51.7	46.9	69.1	57.7	8.9	52.1
		Rain	47.0	72.4	21.6	49.0	40.1	43.0	7.7	40.5	40.1
		Night	33.2	55.8	12.8	33.2	36.4	22.5	17.5	- <sup>†</sup>	30.2
		Fog	39.1	81.5	50.4	65.3	66.3	57.6	63.9	81.0	63.1

<sup>†</sup> No bus instance is available in the ACDC-night validation split.

Cityscapes-to-ACDC. We use Grounding DINO with the Swin-B backbone, identical to that used in DEPF. To ensure fairness given the backbone differences between Swin-B Grounding DINO and ResNet-50 Deformable DETR, we also compare against our method using Swin-B Deformable DETR. Results are reported in Tab.8 and Tab.9.

Benefiting from large-scale pretraining, Grounding DINO achieves strong zero-shot results on diverse weather conditions (e.g., 34.3% mAP on Foggy Cityscapes). However,

by integrating the general visual knowledge from Grounding DINO with the domain-specific knowledge of the source detector, our approach consistently outperforms zero-shot Grounding DINO under the same backbone (e.g., 52.9% vs. 34.3% mAP on Foggy Cityscapes), demonstrating the effectiveness of our method and the advantage of leveraging VFM for SFOD.

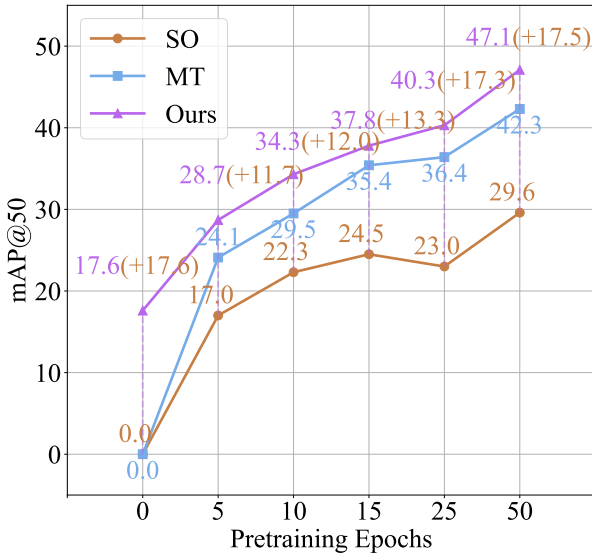


Figure 6: Results of Source-only (SO), Mean Teacher (MT), and ours under restricted pretraining epochs and weak source pretraining performance.

#### D.4 VFM Backbone Selection

We investigate the effect of different Vision Foundation Model (VFM) backbones used in our PGFA and PIFA modules. As summarized in Tab. 10, the choice of VFM significantly influences overall detection performance. Among all configurations, DINOv2 with a ViT-G/14 backbone achieves the highest mAP of 47.1%, with performance constantly improving as the ViT model scale increases from ViT-S to ViT-G. This trend highlights the benefit of stronger semantic representations provided by larger vision transformers, which facilitate more accurate and robust cross-domain alignment.

Interestingly, although Grounding DINO is specifically designed for object detection and integrates multimodal supervision from vision-language data, its performance lags behind DINOv2-based variants—achieving only 46.2% mAP at best with Swin-B. This performance gap may originate from the following reasons: (1) the comparatively smaller pretraining dataset used by Grounding DINO (1.82M images) versus DINOv2 (142M images) (Oquab et al. 2023), which may limit the diversity and generality of its learned features, and (2) the added complexity and potential domain mismatch introduced by vision-language feature spaces in Grounding DINO, which might be less optimal for purely visual alignment tasks like ours.

#### D.5 Pseudo-label Fusion Strategies

We compare multiple pseudo-label fusion strategies to validate DEPF. Tab.10 further reveals that relying solely on either the teacher model or Grounding DINO for pseudo-label generation results in suboptimal performance, underscoring the necessity of integrating predictions from both

Table 10: Performance comparison of different VFM backbone series (left) and pseudo-labeling strategies (right). “RI” means remove individual predictions.

Aligning VFM	Size	mAP	Pseudo labels	mAP
Grounding DINO	Swin-S	46.0	Teacher only	45.0
	Swin-B	46.2	GDINO only	43.3
DINOv2	ViT-S/14	46.2	NMS	46.3
	ViT-B/14	46.7	WBF	46.7
	ViT-L/14	46.8	ours + RI	43.2
	ViT-G/14	47.1	ours w/o weight	46.8
			ours	47.1

Table 11: Computational efficiency analysis. Comparison of training and inference time among the Mean Teacher baseline, PGFA & PIFA (with DINOv2), and DEPF (with Grounding DINO).

Mean Teacher	PGFA & PIFA	DEPF	mAP / Gain	$\Delta$ Training time↑	$\Delta$ Inference time↑
✓			42.3 / -	+0.0%	
✓	✓		45.0 / +2.7	+28.6%	
✓	✓	✓	45.9 / +3.6	+42.8%	+0.0%
✓	✓	✓	47.1 / +4.8	+79.0%	

sources. Naively applying standard fusion methods like Non-Maximum Suppression (NMS) or Weighted Box Fusion (WBF)(Solovyev, Wang, and Gabruseva 2021) also falls short, which yields 0.8% and 0.4% lower mAP than our proposed method, respectively. This performance gap is likely due to two factors discussed in the main paper: the difficulty of tuning confidence weights and the negative impact of contradictory predictions that are not properly processed.

The importance of fusing contradictory predictions is further illustrated by the pseudo-label visualizations in Fig. 8. In line 2 of the figure, the teacher and Grounding DINO assign different labels to the same object by predicting `rider` and `person`, respectively. If vanilla NMS or WBF is directly applied, both predictions may survive and be treated as valid pseudo-labels. This leads to label ambiguity and conflicts during training, ultimately harming optimization.

We also evaluate an alternative fusion strategy, Remove Individual (RI), which discards predictions not shared by both sources. While this approach avoids contradictory labels, it sacrifices recall and suppresses complementary information, resulting in inferior performance.

In contrast, our entropy-aware fusion strategy achieves the best performance (47.1% mAP) by jointly refining both box locations and class logits based on uncertainty. This design not only resolves label conflicts but also leverages the strengths of both sources, leading to improved localization and classification quality.

#### D.6 Computational Efficiency Analysis.

To provide a clearer understanding of the computational overhead introduced by each component, we analyze both training and inference efficiency, as summarized in Tab. 11. PGFA and PIFA are grouped together since they share the same feature extraction backbone from DINOv2, while DEPF relies on Grounding DINO for pseudo-label generation during inference. Compared with the Mean Teacher

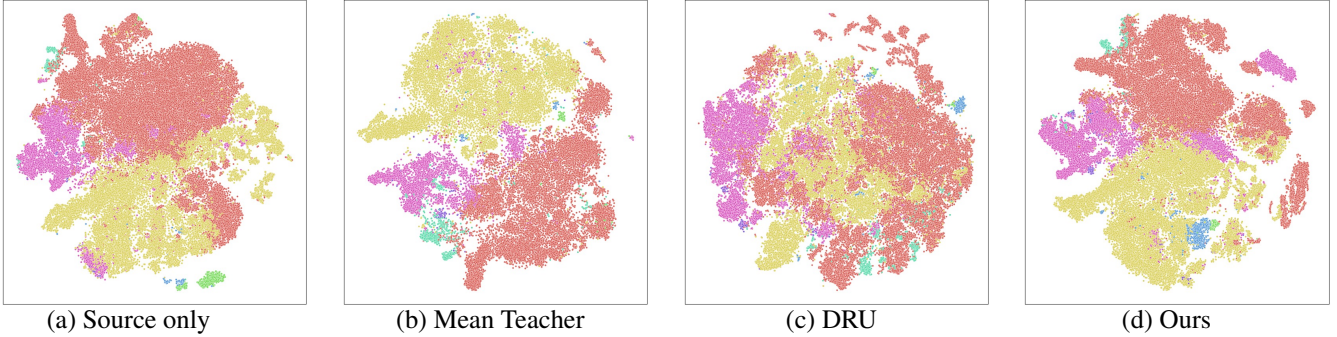


Figure 7: t-SNE visualization of instance-level features colored by predicted categories on the target domain. From left to right: (1) Source only, (2) Mean Teacher baseline, (3) DRU (Khanh et al. 2024), and (4) Ours. Each point represents an instance-level feature, and different colors indicate different predicted classes. Our method produces more compact and well-separated class clusters, indicating enhanced discriminability under domain shift.

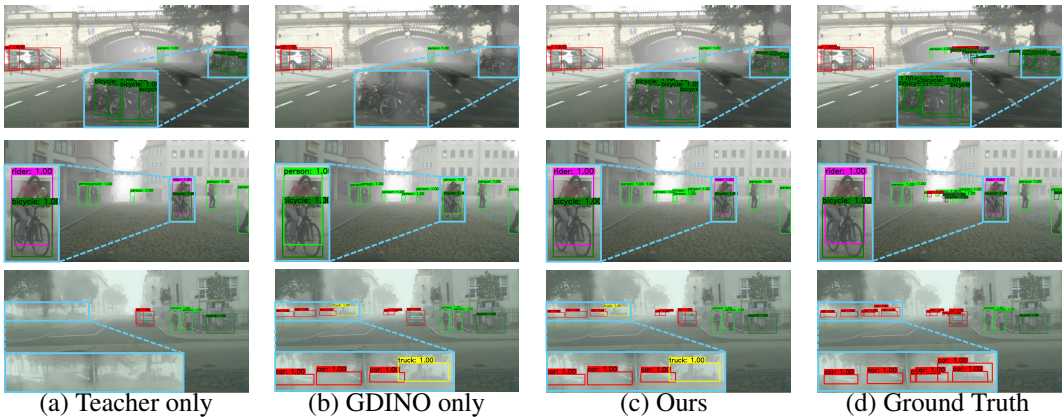


Figure 8: Pseudo-label visualization on the Cityscapes-to-Foggy Cityscapes adaptation scenario among (a) Teacher only, (b) GroundingDINO (GDINO) only, (c) Ours (Teacher+GDINO fused), (d) Ground Truth. We zoom in the discriminative regions for each set of predictions.

baseline, integrating PGFA & PIFA increases training time by 28.6% but brings a 2.7 mAP gain. Incorporating DEPF alone raises training cost by 42.8% while achieving a 3.6 mAP improvement. When all modules are combined, the training overhead reaches 79.0%, yet the overall performance gain is the highest (+4.8 mAP). Notably, the inference time remains unchanged since all VFM are employed solely for offline feature extraction or pseudo-label generation, without introducing additional parameters or modules during inference. This design preserves deployment efficiency and ensures fair comparisons with baseline models.

## D.7 Robustness to Weak Source Pretraining

A key challenge in SFOD is **reliance on high-quality source-pretrained models**, which are often inaccessible due to privacy concerns. We simulate weak pretraining by limiting source model epochs, and we run our SFOD algorithm with the same training epochs and hyperparameters. Results in Fig. 6 show that even with minimal pretraining, our method still provides substantial gains, showing resilience to poor initialization. Notably, even without any source pretraining, our method still achieves 17.6% mAP

under the same number of adaptation epochs. Moreover, stronger source models result in larger performance gains (e.g., +11.7% for 5 epochs, +17.5% for 50 epochs), confirming that effectively leveraging limited source knowledge via VFM is crucial and suggests a promising direction for future research.

## D.8 Failure Case Analysis

Figure 9 presents representative pseudo-label failure cases in the Cityscapes-to-Foggy Cityscapes scenario. In the first row, our fusion mechanism fails to suppress a high-confidence false positive inherited from one source model. Although the complementary model correctly omits this region, the fusion retains the erroneous detection due to the dominant confidence weight, revealing a limitation in filtering model-specific false activations. In the second row, the fused pseudo-label exhibits inaccurate localization, where slight spatial misalignment between the teacher and Grounding DINO boxes leads to a blurred or misplaced fusion result. This indicates that when both sources provide coarse or inconsistent spatial cues, the fusion may propagate localization noise rather than refine it. These observations suggest



Figure 9: Pseudo-label visualization (**failure cases**) on the Cityscapes-to-Foggy Cityscapes adaptation scenario among (a) Teacher only, (b) GroundingDINO (GDINO) only, (c) Ours (Teacher+GDINO fused), (d) Ground Truth.

that while the fusion strategy effectively enhances coverage in most cases, its robustness could be further improved through confidence calibration and geometry-aware alignment.

#### D.9 t-SNE Visualization

To further assess the discriminative capability of our method, we visualize the instance-level features on the target domain using t-SNE (Maaten and Hinton 2008), with color indicating the predicted class. As shown in Fig. 7, the source model (leftmost) exhibits severely entangled class distributions, reflecting its poor generalization to the target domain. The Mean Teacher baseline provides modest improvement, while DRU demonstrates stronger separation in some regions. In contrast, our method yields significantly more compact and clearly separated clusters, suggesting that the features learned through VFM-guided alignment and dual-source supervision are more discriminative and semantically coherent. These visual results align with our quantitative improvements and validate the effectiveness of our approach in enhancing class separability under domain shift.